Aérodynamique d'un micro rotor en environnement confiné

S. PROTHIN[a], T. JARDIN[a], N. DOUE[a], C. FERNANDEZ-ESCUDERO[a]

1. ISAE-Supaéro, Département d'aérodynamique et Propulsion, 10 avenue Edouard Belin, 31055, Toulouse, France

Résumé

Dans le cadre des recherches conduites au sein du département Aérodynamique et Propulsion (DAEP) de l'ISAE, et plus particulièrement l'équipe travaillant sur l'aérodynamique et la propulsion des Micro-Drones s'intéresse à l'aérodynamique de micro-rotors en milieu confiné. L'étude s'inscrit dans le cadre du développement de micro-drones de type indoor destinés, par exemple, à l'exploration de réseaux souterrain (grottes ornées) et/ou l'observation en environnements contraignants (installations nucléaires).

L'enjeu est double, d'une part, évaluer l'influence de parois sur le comportement aérodynamique du micro-rotor, et d'autre part, comprendre l'influence du micro-rotor sur l'environnement proche.

Abstract

As part of the research carried out within ISAE's Aerodynamics and Propulsion Department (DAEP), and in particular the team working on aerodynamics and propulsion of Micro-Drones, is interested in the aerodynamics of micro-rotors in confined environment. The study is part of the development of indoor micro-drones for the exploration of undrground networks (ornate caves) and / or observation in restricted environments (nuclear installations).

The challenge is twofold: firstly, to evaluate the influence of walls on the aerodynamic behavior of the micro-rotor and, on the other hand, to understand the influence of the micro-rotor on the nearby environment.

Mots clefs : Aérodynamique, Rotor, Drone, Confiné, Expérimental, Numérique

1 Introduction

Micro-Air Vehicles (MAVs) have recently gained interest owing to their ability to perform missions of observation at relatively low cost. In response to the 1996-2000 MAV Program initiative by the US Defense Advanced Research Projects Agency (DARPA), three main concepts of MAVs have emerged: fixed-wing, rotary-wing and flapping-wing MAVs (Refs. 1–3). Fixed-wing MAVs are

mostly dedicated to long-range missions due to their relatively long-endurance and high-speed range. However, they are not hovering capable and are hence mostly restricted to outdoor missions.

Conversely, rotary-wing MAVs suffer from low-endurance but offer the possibility to evolve in confined environment due to their ability to perform hovering flight and to achieve enhanced maneuverability. While the two former concepts simply derive from the scaling of conventional aircraft and helicopters, the flapping-wing concept derives from the observation of nature. This alternative bioinspired concept could potentially allow hovering flight, enhanced maneuverability and low noise generation while providing reasonable aerodynamic performance, hence endurance, at low Reynolds numbers typical of insect flight. Although flapping-wing MAVs may appear as a promising concept at several levels, they involve complex mechanical systems and complex aerodynamics that make it an immature technology (Refs. 4–7). Thus, to date, rotary-wing MAVs appear as the most relevant solution for missions of observation in confined environments. While the aerodynamic performance of hovering micro rotors in non-confined environments has been extensively studied (Refs. 8–11), virtually no research work has focused on micro-rotors in highly confined environments. Few studies report results of micro-rotors In Ground Effect (IGE) though, showing that a rotor hovering in the vicinity of the ground outperforms a hovering rotor Out of Ground Effect (OGE). These results are of paramount importance for both the design of efficient auto-pilot and the definition of low-consumption flight strategies (Ref. 12). In this context, Lee et al and Lakshminarayan et al (Refs. 13, 14) have brought to the fore the complexity of the flow that develops around an IGE micro-rotor using PIV measurements and URANS computations respectively. Nathan et al (Ref. 15) have experimentally investigated the flow around an IGE micro-rotor both hovering in crosswind and in forward flight. On the basis of PIV measurements, the authors have highlighted differences between the two configurations in the transition from recirculation regime to ground vortex regime. In another context, still using IGE micro-rotors, various authors motivated by the necessity to augment knowledge on the brownout phenomenon have unraveled the prominent flow features that promote upliftment of sediment particles (Refs. 16–18).

Overall, the aforementioned studies demonstrate that boundary conditions are critical to the aerodynamic performance of micro-rotors as they may significantly constrain the development of the rotor wake. In this paper, we extend previous works to the experimental analysis of lateral and upper wall effects, as well as channel and duct effects. These configurations modelize highly confined environments that may be encountered by an MAV performing indoor reconnaissance. In particular, we show that ceiling effects have a beneficial impact on aerodynamic performance, in a rather a similar way to that obtained in ground effects yet through a distinct physical mechanism. Furthermore, channel effects seem to derive from a simple linear combination of both ceiling and ground effects. In contrast, lateral walls have negligible effects on aerodynamic performance whether they are isolated or in duct configuration. All these observations help raise guidelines for the design of efficient auto-pilot.

2 Experimental Setup

An illustration of the experimental setup is shown in **figure 1**. The micro-rotor has a radius R=125 mm and consists of two untwisted flat plates with a 15 degrees pitch angle. For each case, the rotor was powered using an AXI 2808/24 goldline brushless motor. A PID controller was implemented in order to operate the rotor at rotational frequencies ranging from 20 to 60 Hz within +/ 1% accuracy. Variations in rotational frequencies allowed to keep the rotor thrust constant for different rotor-to-boundaries distances. The rotor was operated such that its tip-path-plane was parallel and/or perpendicular to wall boundary conditions, depending on the configuration considered. It was connected via a 600 mm long steel beam to a mechanical traverse that allowed to automatically adjusting the rotor-to-boundaries distance. Wall boundaries consisted of 900_900 mm2 (roughly 7.2x7.2 R^2) Plexiglas (ground plane) and wooden (upper and side walls) plates. The rotor was mounted on an offset balance that allowed two force components and three torque components to be measured within +/-1% accuracy. The maximum range of the balance was 10 N and 0.5 Nm for force

and torque measurements respectively. Mean forces and torques were obtained by averaging 5000 samples acquired at a frequency of 1 kHz over a time interval of 5 s. For each case, four runs were performed to assess the repeatability of the load measurements. Results presented in this paper were obtained by averaging the values of the repeatability runs. Note that data obtained with the motor mounted upstream and downstream of the rotor (to allow small gaps between the rotor and the boundaries) overlapped within the error margin. In addition, velocity flow fields in the axial plane of the rotor were obtained through high-definition stereoscopic Particle Image Velocimetry (PIV) measurements. Two FlowSense EO 16M cameras were synchronized to a 2x200 mJ DualPower Bernoulli laser and driven via Dynamic Studio (Dantec) commercial software. While the laser was operated at a nominal 15 Hz frequency, PIV images were acquired at 2.5 Hz (every six laser impulse) due to the maximum 2.6 Hz allowable operating frequency of the cameras. The laser power was set to 35 mJ in order to limit laser reflections on the rotor and the walls. The cameras were equipped with a 85 mm focal length Samyang lens, F/4. The time step between two images used for the cross-correlation was set to 80 ms. Velocities were computed using an adaptive cross-correlation (two refinement steps) with a final window size of 16x16 px², and spurious velocities were identified using a peak ratio validation procedure (with a peak-to-peak ratio of 1.2). The final dimensions of the reconstructed three-component flow fields were approximately 600x400 mm2 (4.8x3.8 R²), leading to a spatial resolution of 0.25 mm (2.10^{-3} R). For each case, 1000 instantaneous velocity flow fields were averaged, ensuring convergence of both mean and fluctuating values. In what follows, all velocities are non-dimensionalized using the induced velocity v_i derived from rotor thrust measurement T and momentum theory: $v_i = [T / 2\rho\pi R^2]^2$.

3 Results

This section aims at understanding how horizontal and lateral wall boundary conditions affect the aerodynamic performance of micro-rotors. Toward that end, we focus on the evolution of the Power Loading (PL) as a function of the non-dimensional distance h/R that separates the center of the rotor disk from the wall, at a given Disk Loading (DL). Recall that PL is defined as the ratio between the thrust and the power of the rotor $T/Q\omega$, and that DL is defined as the ratio between the thrust and the area of the rotor disk T/A, with $A=\pi R^2$. The $PL=f(h/R)_{DL}$ curve is of paramount importance in practice as it reveals the enhancement or degradation of the aerodynamic performance of a given MAV as it approaches horizontal or lateral walls.

Ground Effect

Figure 2 displays the evolution of the ratio of the power loadings obtained in and out of ground effects as a function of the rotor to ground distance h/R, at a given DL. It is shown that $PL_{IGE}=PL_{OGE}$ is roughly constant for values of h/R above 2 but rapidly increases for values of h/R below 2, as h/R tends to 0.

This trend, which is extensively reported in the literature, is associated with the radial expansion of the rotor jet. Such a phenomenon is illustrated on figure 3 which depicts streamlines and fluctuating radial velocity isolines superimposed to velocity magnitude isocontours for both h/R=1 and h/R=2 IGE cases.

Overall, it is shown that the rotor jet expands radially, away from the rotor axis where a strong recirculation region develops. In the h/R=2 case, the recirculation region in the vicinity of the ground is sufficiently far away from the rotor disk to allow for a slight contraction of the jet immediatly downstream of the rotor hub before the flow is constrained to circumvent the recirculation region in the outward direction. In the h/R=1 case, the recirculation region is tilted along the rotor axis direction and fills the gap between the rotor and the ground, preventing any jet contraction. Here, the flow is severely constrained in the outward direction immediately after the rotor disk. This simple comparison between the h/R=1 and h/R=2 cases thus shows that the jet expansion is more pronounced for low values of h/R.

The influence of ground proximity on jet expansion is further highlighted on **figure 4** which shows the periphery of the jet for different h/R cases. The periphery of the jet is here extracted from local maxima of radial velocity fluctuations. It clearly appears that jet expansion increases with

decreasing values of h/R, with a minimum jet section roughly ranging from 0.78A at h/R=1 to 0.61A at h/R=4. In addition, such an expansion is correlated with a reduction and homogenization of the axial velocity at the rotor disk. This is highlighted on **figure 4** which depicts spanwise profiles of axial induced velocity at the rotor disk. This mechanism, together with a reduction in tip vortex strength, is known to promote aerodynamic efficiency (Ref. 19). Overall, three main features can be observed: 1) axial velocity along most of the blade span is reduced, 2) maximum axial velocity is reduced and moved towards the wing tip, 3) negative velocities are induced at the blade root due to the interaction with the recirculation region.

The increase in $PL_{IGE}=PL_{OGE}$ with decreasing h/R values can also be viewed as an increase in thrust at a given power. This extra lift when approaching the ground is appreciated by helicopter pilots as it contributes to secure landing phases.

In the framework of MAVs, another interest emerges; that of significantly reducing power consumption and hence increasing flight endurance when flight is performed IGE. In other words, an interesting strategy to enhance MAVs endurance is to allow for robust IGE flight. This requires to promote flight robustness through the definition of simple models dedicated to auto-pilot design. As such, **figure 2** shows that empirical asymptotic models of the form :

$$\mathbf{a \times (h/R\hat{}) ^{-0.55} + b}$$

provide a reasonable estimation of the evolution of $PL_{IGE}=PL_{OGE}$ as a function of h/R. Furthermore, it is interesting to note that the evolution of $PL_{IGE}=PL_{OGE}$, hence the model, is roughly independent to DL.

Ceilling Effect

While it is known that MAVs endurance can significantly benefit from IGE flight phases, we here ask if MAVs can benefit from flight phases In Ceiling Effects (ICE)? The literature on rotors being historically associated with the study of manned helicopters, and the latters being not confronted to ICE flight phases in practice, this MAVs-specific flight configuration is virtually undocumented.

Similarly to the IGE case, **figure 5** shows the evoultion of the $PL_{ICE}=PL_{OGE}$ ratio as a function of the rotor to ceiling distance h/R, at a given DL. A prominent feature is the drastic increase in $PL_{ICE}=PL_{OGE}$ as h/R tends to 0. This increase is stronger than that observed in the IGE case, with values of PLICE=PLOGE reaching 2.55 at h/R=0.12 (to be compared with the value of 1.56 at h/R=0.12 in the IGE case). Furthermore, ceiling effects occur at lower values of h/R than IGE effects and thus appear as a more sudden and severe phenomenon.

Conversely to the IGE case, the increase in $PL_{ICE}=PL_{OGE}$ for decreasing values of h/R is not related to any jet expansion. Rather, the proximity of the ceiling restricts the axial incoming flow above the rotor, which is to be compensated by the development of a radial incoming flow. This feature is visible on **figure 6** which depicts streamlines and fluctuating radial velocity isolines superimposed to velocity magnitude isocontours for both h/R=1 and h/R=2 ICE cases.

Furthermore, **figure 7** shows that the proximity of the ceiling and the restriction in axial incoming flow above the rotor does not significantly alter the axial induced velocity at the rotor disk, despite a reduction in maximum axial velocity magnitude. This suggests that the prominent mechanism that leads to an increase in aerodynamic performance is different from that occuring in IGE configurations. Here, as previously mentionned, it can be seen that the rotor feed air comes from aside, and even from beneath of the rotor. As the section between the rotor and the ceiling decreases, the flow increasingly distortsand accelerates towards the rotor. The flow pattern recalls that in a constricted pipe section, which is conducive to venturi effects. Correlating this to the evolution of $PL_{ICE}=PL_{OGE}$ as a function of h/R indicates that the rotor is sucked to the ceiling for sufficiently low values of h/R, making it a sudden and severe phenomenon. Besides, although this mechanism differs from that observed in IGE configurations, it should be noted that the reduction in tip vortex strength due to wall proximity is common to both IGE and ICE cases. Overall, three main features can here again be observed: 1) axial velocity along most of the blade span is unchanged, 2) maximum axial velocity is reduced, 3) upward velocities are induced outside the rotor due to distortion in rotor feed air.

These results show that ICE flight is more beneficial to MAVs endurance than IGE flight is, providing that the MAVs auto-pilot is sufficiently robust to allow for ICE flight with very low h/R values. Therefore, there is a significant interest in defining models that contribute to auto-pilot robustness for ICE flight. As such, **figure 5** shows that asymptotic models of the form :

$$\mathbf{a \times (h/R\hat{}) ^{-1,23} + b}$$

can provide a reasonable estimation of the evolution of $PL_{ICE}=PL_{OGE}$ as a function of h/R.

Channel Effect

In this subsection, we focus on the effects of channel-type confinement on the aerodynamics of micro-rotors (IChE). Channel configuration results from the combination of IGE and ICE configurations and opens the path towards the study of highly confined configurations typical of indoor flight (e.g. intrusion through vent pipe or underground tunnels). More specifically, in light of previous results, we ask if IChE aerodynamic performance simply results from the linear combination of IGE and ICE aerodynamic performance or if strong non-linear coupling tend to generate a completely new scenario.

The distance H between the lower (ground) and upper (ceiling) horizontal walls is introduced.

Figure 8 shows the evolution of the $PL_{IChE}=PL_{OGE}$ ratio as a function of the rotor to ground distance h/R, at a given DL and for H/R=4. The evolutions of $PL_{IGE}=PL_{OGE}$ and $PL_{ICE}=PL_{OGE}$ are added for ease of comparison. Interestingly, and somehow counter-intuitively, the results indicate that the IGE and ICE effects coupling can in a first approach be treated as a linear coupling.

This observation is further highlighted on **figure 9**. Overall, it can be seen that the global flow structure above the rotor is roughly similar to that of the ICE case while the global flow structure below the rotor is roughly similar to that of the IGE case. In some way, the rotor acts as an impermeable frontier that makes the downstream flow independent to the upstream conditions and vice versa. Although this statement is reasonably valid for prominent steady flow features, it should be noticed that IChE configurations enhance flow unsteadiness, with higher levels of velocity fluctuations. Unsteady data would be required to determine if unsteady phenomena are likely to occur at a time scale that is detrimental to MAVs attitude control.

Nonetheless, showing that IChE effects result from the quasi-linear combination of IGE and ICE effects, at least in a mean sense, is conducive to flight robustness in confined environments and provides simple guidelines for the definition of robust auto-pilot.

Wall effects

We finally address the influence of lateral wall proximity on the aerodynamics of micro-rotors (IWE). On the contrary to previous cases, wall effects break the symmetry of the problem as they influence a limited portion of the rotor disk. In this particular case, it is observed that the $PL_{IWE}=PL_{OGE}$ ratio is not significantly affected by wall proximity (and is therefore not shown here). On the other hand, **figure 10** shows that the flow structure is modified. As the rotor to wall distance decreases, the rotor jet is sucked towards the wall, which tilts its axis in the counter-clockwise direction. In addition, the tip vortex is flattened in the vertical direction and its strength is significantly reduced when approaching the wall. Both wake tilting and changes in tip vortex size and strength naturally induce a lateral force and a rolling moment that is however too weak to be measured here. Flow modifications induced by the proximity of the wall are localized within a small portion of the rotor disk which makes their influence on aerodynamic loads negligible. Obviously, this is no more true if the rotor disk is slightly tilted, i.e. if the rotor disk is not strictly perpendicular to the wall and the rotor jet impinges the wall, which is a common feature of advancing rotating wing MAVs. Therefore, for missions in confined environments, there is a significant interest in developing robust attitude control that prevent rotor tilting when performing forward flight towards vertical walls. Furthermore, additional results have shown that In Duct Effects (IDE), which result from the presence of two parallel lateral walls from both sides of the rotor, do not significantly influence aerodynamic loads either. Note that such results were obtained for values of y/R as low as 0.55.

4 Conclusion

Due to their small dimensions, micro-air vehicles offer the possibility to perform missions of reconnaissance in confined environments. Search & rescue task forces, archeologists and nuclear security workforces, to name a few, could greatly benefit from MAVs capable of robust indoor flight. In this context, a way to enhance flight robustness is to understand how the rotor of a hovering capable MAV responds to wall proximity in terms of aerodynamics performance.

Toward that end, we conducted experiments on a micro-rotor hovering in the vicinity of horizontal and vertical walls. By means of force and PIV measurements, we were able to reveal changes in aerodynamic performance due to wall proximity and correlate it with the occurrence of specific flow phenomena. Our results are in line with extensive research on ground effects, showing that aerodynamic performance benefits from ground proximity due to a reduction in induced axial velocity at the rotor disk and reduction in tip vortex strength. In addition, while ceiling proximity also leads to an enhancement of aerodynamic performance, it is shown that ceiling effects are more severe and sudden than ground effects and can be viewed as Venturi effect acting above the rotor disk. Furthermore, it can be seen that channel effects can quite surprisingly be considered as a linear combination of both ground and ceiling effects. Conversely, vertical wall proximity does not have a major impact on aerodynamic performance, whether an isolated wall or a duct configuration is considered.

These results demonstrate that simple models can be derived for the definition of efficient auto-pilots, contributing to indoor flight robustness. However, to gain further insight into the aerodynamic response of a rotor hovering near wall boundary conditions, dynamic tests will be conducted in the future.

References

[1] Mueller, T.J., and DeLaurier, J.D., ”Aerodynamics of Small Vehicles”, Annu. Rev. Fluid Mech., Vol. 35, 2003, pp. 89-111.

[2] Torres, G.E., and Mueller, T.J., ”Low Aspect Ratio Aerodynamics at Low Reynolds Numbers”, AIAA J., Vol. 42, No. 5, 2004, pp. 865-873.

[3] Pines, D.J., and Bohorquez, F., ”Challenges Facing Future Micro-Air-Vehicle Development”, J. Aircraft, Vol. 43, No. 2, 2006, pp. 290-305.

[4] Dickinson, M.H., Lehmann, F.O., and Sane, S.P., ”Wing Rotation and the Aerodynamic Basis of Insect Flight”, Science, Vol. 284, No. 5422, 1999, pp. 1954-1960.

[5] Platzer, M.F., Jones, K.D., Young, J., and Lai, J.C.S., ”Flapping Wing Aerodynamics: Progress and Challenges”, AIAA J., Vol. 46, No. 9, 2008, pp. 2136-2149.

[6] Shyy, W., Aono, H., Chimakurthi, S.K., Trizila, P., Kang, C.K., Cesnik, C.E.S., and Liu, H., ”Recent Progress in Flapping Wing Aerodynamics and Aeroelasticity”, Prog. Aerospace Sci., Vol. 46, No. 7, 2010, pp. 284-327.

[7] Jardin, T., Farcy, A., and David, L., ”Three Dimensional Effects in Hovering Flapping Flight”, J. Fluid Mech., Vol. 702, 2012, pp. 102-125.

[8] Ramasamy, M., Lee, T.E., and Leishman, J.G., ”Flowfield of a Rotating-Wing Micro Air Vehicle”, J. Aircraft, Vol. 44, No. 4, 2007, pp. 1236-1244.

[9] Ramasamy, M., Johnson, B., and Leishman, J.G., ”Understanding the Aerodynamic Efficiency of a Hovering Microrotor”, J. Am. Helicopter Soc., Vol. 53, No. 4, 2008, pp. 412-428.

[10] Bohorquez, F., ”Rotor Hover Performance and System Design of an Efficient Coaxial Rotary Wing Micro Air Vehicle”, Ph.D. Dissertation, Department of Aerospace Engineering, Univ. of Maryland, College Park, MD, 2007.

[11] Lakshminarayan, V.K., and Baeder, J.D., ”Computational Investigation of Microscale Coaxial-Rotor Aerodynamics in Hover”, J. Aircraft, Vol. 47, No. 3, 2010, pp. 944-950.

[12] Powers, C., Mellinger, D., Kushleyev, A., Kothmann, B., and Kumar, V., ”Influence of Aerodynamics and Proximity Effects in Quadrotor Flight”, Springer Tracts in Advanced Robotics, Vol. 88, 2013, pp. 289-302.

[13] Lee, T.E., Leishman, J.G., and Ramasamy, M., ”Fluid Dynamics of Interacting Blade Tip Vortices with a Ground Plane”, J. Am. Helicopter Soc., Vol. 55, No. 2, 2010, pp. 22005.

[14] Lakshminarayan, V.K., Kalra, T.S., and Baeder, J.D., ”Detailed Computational Investigation of a Hovering Microscale Rotor in Ground Effect”, AIAA J., Vol. 51, No. 4, 2013, pp. 893-909.

[15] Nathan, N.B, and Green, R.B., ”The flow around a model helicopter main rotor in ground effect”, Exp. Fluids, Vol. 52, 2012, pp. 151-166.

[16] Johnson, B., Leishman, J.G., and Sydney, A., ”Investigation of Sediment Entrainment Using Dual-Phase, High-Speed Particle Image Velocimetry”, J. Am. Helicopter Soc., Vol. 55, No. 4, 2010, pp. 042003.

[17] Sydney, A., and Leishman, J.G., ”Measurements of Rotor/ Airframe Interactions in Ground Effect Over a Sediment Bed”, 69th Annual Forum of the American Helicopter Society, Phoenix, Arizona, 2013.

[18] Rauleder, J., and Leishman, J.G., ”Particle-fluid interactions in rotor-generated vortex flows”, Exp. Fluids, Vol. 55, 2014, pp. 1689.

[19] Leishman, J. G., Principles of Helicopter Aerodynamics, Cambridge University Press, New York, NY, 2000, Chapter 10.

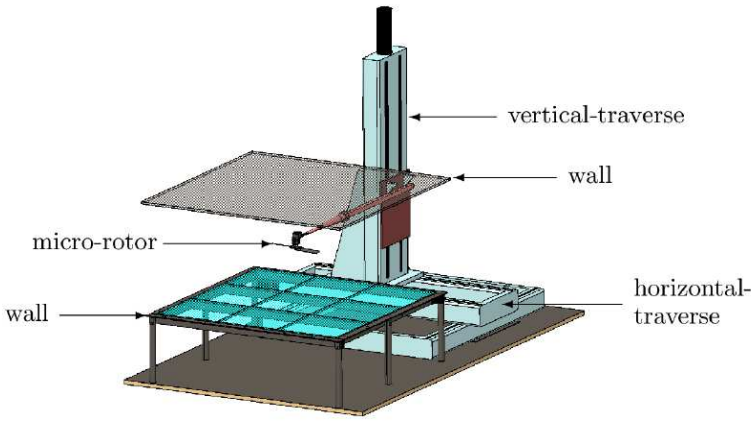

Figure 1. Illustration of the experimental setup

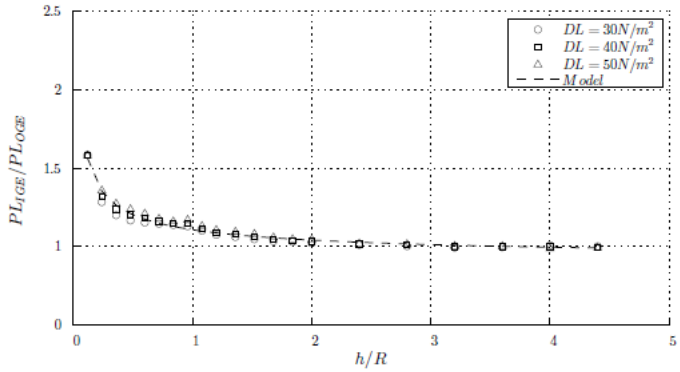

Figure 2. PL_{IGE}=PL_{OGE} ratio as a function of the nondimensional rotor-to-ground distance h/R.

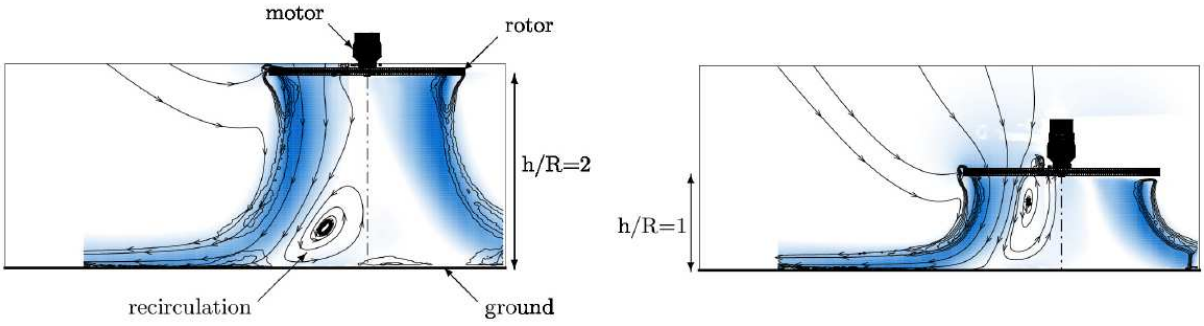

Figure 3. Streamlines and iso-lines of radial fluctuating velocities superimposed to contours of velocity magnitude. Flowfields obtained for the h/R=2 (left) and h/R=1 (right) IGE configurations.

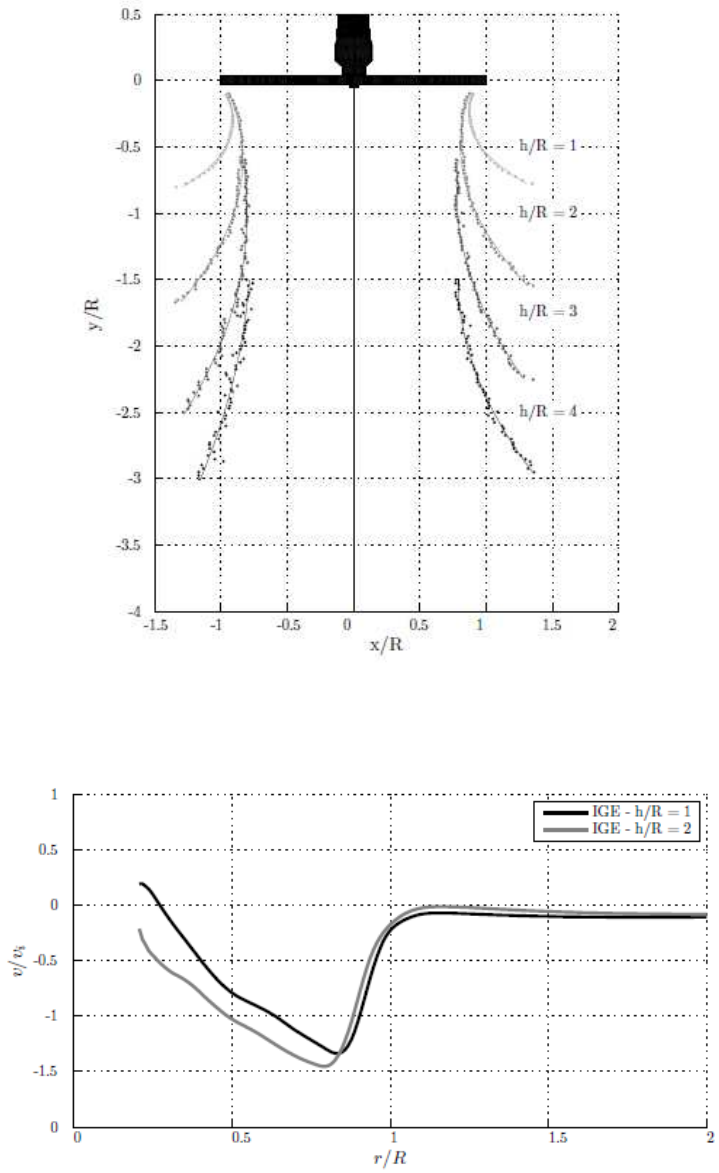

Figure 4. Location of the rotor jet periphery deduced from local maxima of radial velocity fluctuations (top) and nondimensional axial velocity at the rotor disk (bottom) for the IGE configurations.

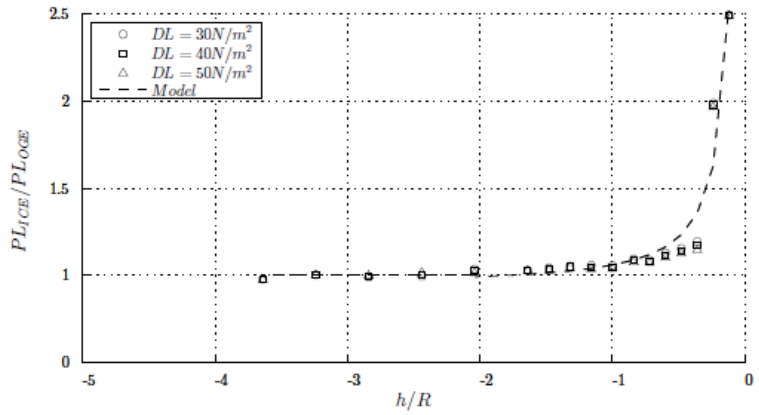

Figure 5. PL_{ICE}=PL_{OGE} ratio as a function of the nondimensional rotor-to-ceiling distance h/R.

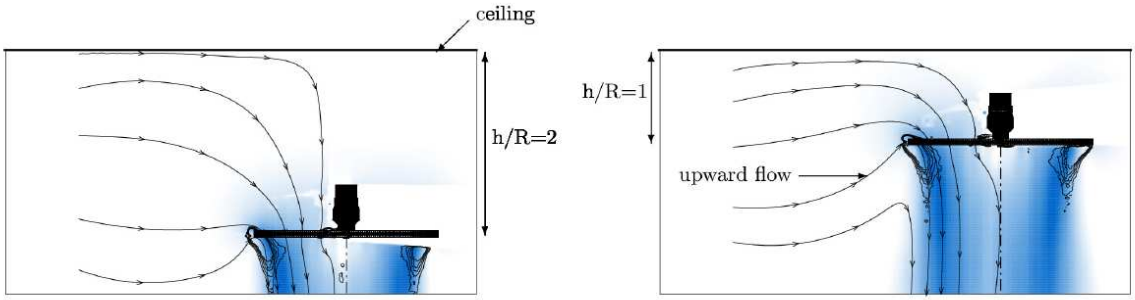

Figure 6. Streamlines and iso-lines of radial fluctuating velocities superimposed to contours of velocity magnitude. Flowfields obtained for the h/R=2 (left) and h/R=1 (right) ICE configurations.

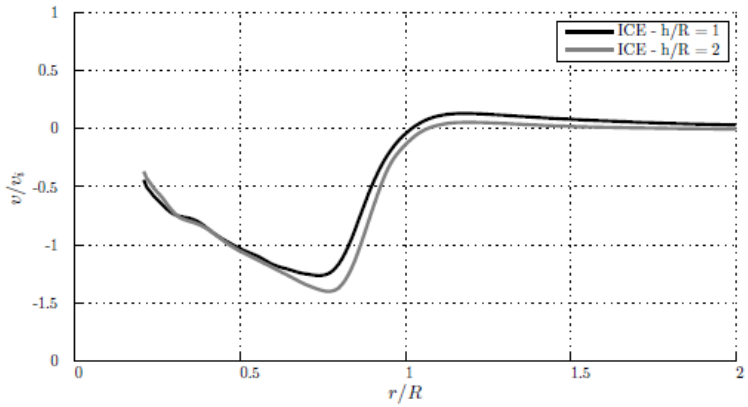

Figure 7. Non-dimensional axial velocity at the rotor disk for the ICE configurations.

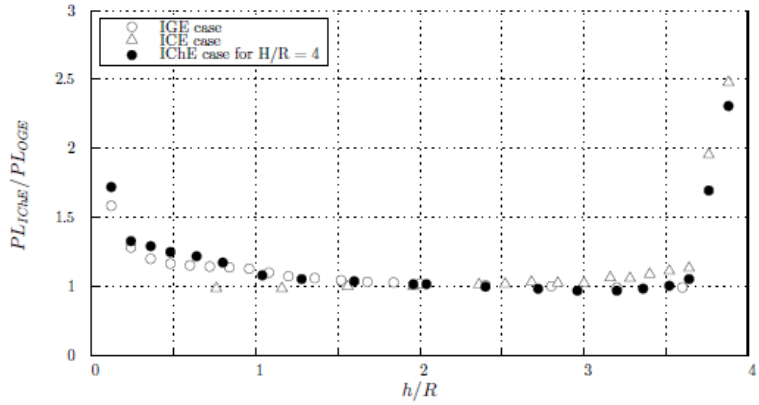

Figure 8. PL_{IChE}=PL_{OGE} ratio as a function of the non-dimensional rotor-to-ground distance h/R, with H/R=4.

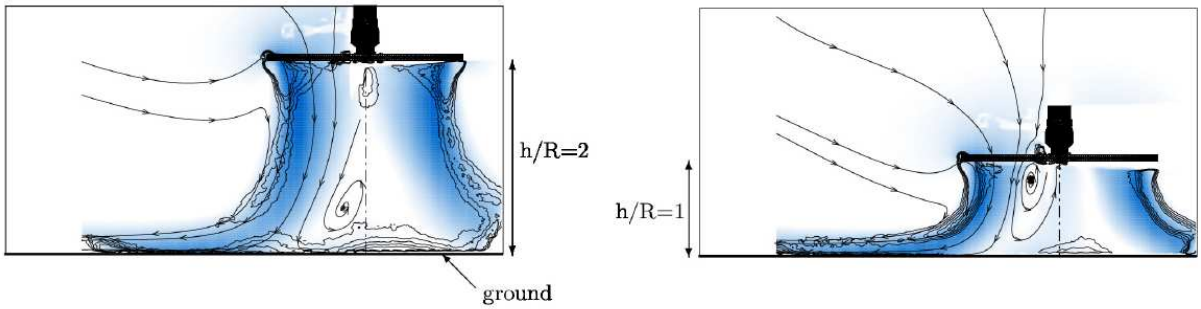

Figure 9. Streamlines and iso-lines of radial fluctuating velocities superimposed to contours of velocity magnitude. Flow fields obtained for the h/R=2 (left) and h/R=1 (right) IChE configurations.

Figure 10. Streamlines and iso-lines of radial fluctuating velocities superimposed to contours of velocity magnitude. Flow fields obtained by PIV for the y/R=0.75 (left) and y/R=0.55 (right) IWE configurations.